Polarized Photoluminescence Excitation Spectroscopy of Single-Walled Carbon Nanotubes

J. Lefebvre and P. Finnie

Institute for Microstructural Sciences, National Research Council, Montreal Road, Ottawa, Ontario, K1A OR6, Canada

(Received 11 January 2007; published 19 April 2007)

The polarized photoluminescence excitation spectra of twenty-five single-walled carbon nanotube species are reported. For light polarized along the nanotube axis, the main absorption resonance at E_{22} shows sidebands attributed to phonon assisted absorption. Sidebands to E_{11} have a diameter dependent energy and are assigned to excited excitonic states. Along with longitudinal excitations, several transverse excitations are identified. The transverse E_{12} resonance has a specific family pattern with energy close to E_{22}. Comparison with theory provides an estimate of the strength of the Coulomb interaction.

DOI: 10.1103/PhysRevLett.98.167406 PACS numbers: 78.67.Ch, 78.55.−m, 81.07.−b

The effective isolation of single-walled carbon nanotubes (SWNTs) from their environment led to the earliest observations of SWNT photoluminescence (PL) [1,2]. The PL process was initially described as free-carrier recombination at the electronic band gap (E_{11}) after light absorption, primarily at a strongly resonant excited state (E_{22}). Interest in the optical properties of SWNTs has since grown, and notably there are significant deviations from the predictions of simple models. As a one-dimensional system, strong Coulomb interaction effects are expected. Although the nature of electron-hole pairs was not readily apparent from early PL experiments, it is now understood that interactions make them excitonic as seen in two-photon absorption experiments [3,4] and theoretical modeling [5–8]. Also, models with or without excitonic effects predict additional states other than E_{11} and E_{22}. Detailed spectroscopic study is necessary to determine their energy and spectral characteristics, and so draw a more complete physical picture of SWNTs electronic structure and the role of Coulomb interactions.

We used PL imaging [9] to identify individual SWNTs and, by tuning the excitation wavelength, obtain their excitation spectrum. Since these SWNTs are straight and spatially resolved, the excitation can be polarized arbitrarily with respect to the tube axis, allowing for unambiguous separation between longitudinal and transverse resonances. Furthermore, because the SWNTs are long, by integrating PL intensities spatially along the length of the SWNT weak absorption resonances are readily detected, even in the case of transverse resonances which are weakened by the depolarization effect [10].

For longitudinal excitation, the main E_{22} resonance was accompanied by weaker resonances, some assigned to phonon sidebands of E_{22}, and others to excited excitonic states of E_{11}. Those latter states have energy close to the calculated exciton binding energy, and are likely due to absorption into the E_{11} continuum. For transverse excitation, a dominant resonance assigned to the E_{12} exciton has a specific family pattern, with energy close to E_{22}. The position of E_{12} is consistent with the exciton picture and allows an estimation of the Coulomb interaction strength.

SWNTs suspended above a patterned silicon substrate were grown by chemical vapor deposition (ethanol vapor with Co catalyst film). We imaged the PL from SWNTs with a 320×256 InGaAs photodiode array (sensitivity from 0.9 to 1.6 μm) [9]. Such images allowed to select SWNT segments (>10 μm) necessary to perform polarized excitation experiments. To minimize bundling effects, a low SWNT coverage sample was used, and only SWNTs that appeared isolated in imaging were selected. PL was excited with a tunable laser with its polarization rotated using a half-wave plate (Ti:sapphire continuous wave, $\sim$720–1020 nm, 100 W/cm^2, 80 μm diameter spot size). For a given SWNT, typically 135 PL images (2.2 nm sampling resolution) were acquired to cover the spectral range of the laser. E_{11} was measured by acquiring an emission spectrum (laser tuned to E_{22}) through a second collection path equipped with a grating spectrometer and a 1024×1 extended InGaAs photodiode array (sensitivity from 1–2.2 μm).

A PL image of an $\sim$80 μm long (15,2) SWNT segment is shown in Fig. 1(a) (SWNT length was typically 10–20 μm). The three dark spots along this SWNT come from PL quenching where the SWNT is supported by the SiO_2 surface. In order to build an excitation spectrum, the intensity from a given SWNT image is integrated for each excitation wavelength of the laser. Figure 1(b) shows the longitudinal (continuous and dashed blue lines) and transverse (continuous red line) excitation spectra for the SWNT in Fig. 1(a). For longitudinal excitation (polarization along the SWNT axis), the spectrum is plotted twice: once to show weaker features (solid blue line) and once to show the overall lineshape (dashed blue line, intensity divided by four). The longitudinal spectrum is dominated by absorption at E_{22} [818 nm in Fig. 1(b)]. The assignment of the weaker features will be discussed in subsequent figures.

For transverse excitation (polarization perpendicular to the SWNT axis), the spectrum shows greatly reduced absorption intensity. On the basis of selection rules, transverse excitations are allowed, but they should be strongly suppressed because of the SWNT geometrical anisotropy

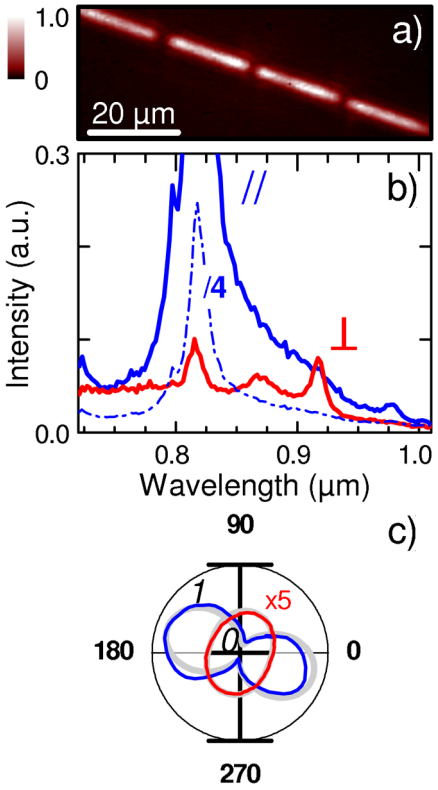

FIG. 1 (color online). Polarized excitation spectroscopy of SWNTs from PL imaging. (a) PL image of a (15,2) SWNT excited at 818 nm. (b) PL excitation spectra for the SWNT in Fig. 1a for laser excitation polarized parallel (continuous blue line) and perpendicular (continuous red line) to the SWNT axis. The dashed blue line shows the same parallel polarization data, with the intensity divided by four. (c) PL intensity versus polarization angle of the laser excitation. Data taken at $E_{22} =$ 818 nm (blue) and $E_{12} = 917$ nm (red). The gray lines are $\cos^2\theta$ functional form.

and the depolarization effect it produces [10]. Still, resonances (at 872 and 917 nm) not visible for the longitudinal case are present in the transverse spectrum. We assign the dominant 917 nm resonance to the E_{12} transition. Measurement of the E_{12} resonance was reported recently for an ensemble of small diameter SWNTs [11]. Further confirming its transverse nature, Fig. 1(c) shows the polarization dependence taken at 818 nm (the E_{22} resonance) and 917 nm (the E_{12} resonance, multiplied by five). For E_{22}, the absorption is strongly polarized along the SWNT axis while for E_{12}, it is transversely polarized. In both cases, the polarization dependence is well fitted using a $\cos^2\theta$ functional form with a 90° phase difference between the two [thick gray lines in Fig. 1(c)].

We have identified longitudinal and transverse resonances for twenty-five (n, m) species (See supplementary material [12] for excitation and emission spectra). The E_{11} emission has the characteristics asymmetric line shape with linewidth in the 9–10 meV range. The line shape and linewidth for E_{22} vary significantly with a typical width around 40 meV and a spread from 30 to 50 meV. For E_{12}, we find a typical linewidth of 20–25 meV with values between 15 and 30 meV. If lifetime broadening determines the linewidth, this indicates that E_{12} excitations decay more slowly than E_{22} excitations.

The loci of E_{11} and E_{22} are plotted in Fig. 2(a) for more than 70 individual SWNTs studied in this work. The thick gray lines in Fig. 2(a) are empirical fits as in Ref. [13]. In contrast with an earlier result by our group [14], inhomogeneous broadening was observed in this sample. Because near zigzag SWNTs of a given family [defined by $2n + m$; see labels in Fig. 2(a)] have similar E_{11} and E_{22} energies, inhomogeneous broadening precludes unambiguous assignment of those species. The origin of the inhomogeneity is unclear, but it is sufficiently small as to have no effect on the conclusions of this work.

The energy of the main transverse resonance (E_{12} exciton) is plotted in Fig. 2(b) as a function of E_{11} energy. Its energy is lower than, but close to the corresponding E_{22} resonance. The family pattern in Fig. 2(b) can be fitted using the same empirical formula as for E_{11} and E_{22}, but with different parameters [12]. While the magnitude of the chiral dependent term differs significantly from the mod1 to the mod2 family for E_{11} and E_{22}, it is mod independent for E_{12}.

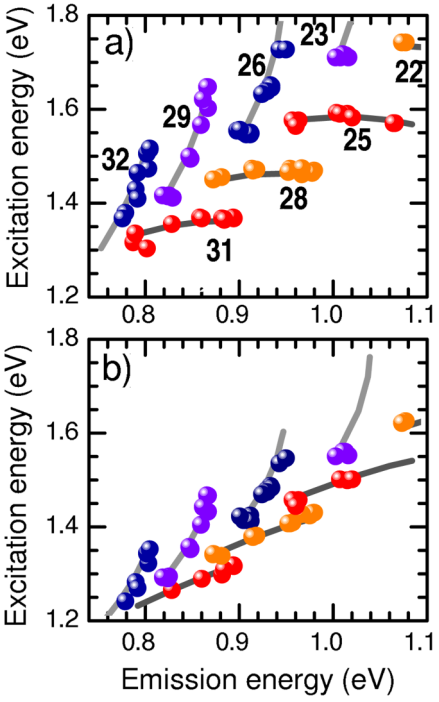

FIG. 2 (color online). Main resonance observed for longitudinal and transverse excitation. (a) E_{22} resonance energy versus E_{11} emission energy. Red and orange circles are for SWNT species with mod$(n - m, 3) = 2$ (or simply mod2) and navy and purple for mod1. The thick continuous gray lines were obtained from an empirical fit (see supplementary material). (b) E_{12} resonance energy versus E_{11} emission energy. Labeling is the same as Fig. 2a.

In a noninteracting picture, the E_{12} (or alternatively E_{21}) transition connects states from the valence and conduction bands that differ by one quantum of angular momentum. In the simplest approximation where electron-hole symmetry is assumed, two degenerate transitions E_{12} and E_{21} are expected halfway between E_{11} and E_{22}. In reality, carrier hoping between the two carbon sublattices produces a modest energy splitting [15]. In this work, the strongest transverse resonance and also lowest in energy is assigned to E_{12} (E_{12} and E_{21} are not distinguished here). These experimental E_{12} values deviate from the simpler predictions ($E_{12} = 0.5E_{22} + 0.5E_{11}$), and are closer to $0.8E_{22} + 0.2E_{11}$. Using $E_{12} = (1 - x)E_{22} + xE_{11}$, we find that x ranges from 0 and 0.25, with a simple functional dependence on $\cos(3\alpha)/d$.

Compared to noninteracting pictures, Coulomb interaction introduces different excitonic corrections to all single particle bands, and it is predicted that E_{12} should lie close to E_{22} [8,16]. Reference [16] provides a fair estimate of E_{12}, E_{11} and E_{22} energies when γ_o is set to 2.6 eV, and U around $0.07\gamma_o$ (γ_o is related to the band parameter, and $U \sim 0.07\gamma_o = 0.18$ eV where U is the strength of the Coulomb interaction) [17]. This model however, has no chiral angle dependence. In contrast with the noninteracting picture where two resonances are expected, the excitonic picture predicts only one dominant resonance [8].

Several weaker sidebands to E_{22}, E_{11} and E_{12} were identified for both polarizations, and their positions are marked in the supplementary material. The position of three sidebands to E_{22} is plotted in Fig. 3(a) on a plot of their energy versus E_{22}. One is clearly a straight line (G label), another shows a smooth functional dependence (s label), and another is most likely a straight line ($2G$ label). With a 200 meV rigid offset with respect to E_{22}, one sideband can be assigned to a phonon (the G-sideband phonon is expected at 197 meV) assisted process [18]. This resonance appears broader and at least 10 times weaker than the main E_{22} resonance. The first G-sideband overtone is visible in three cases ($2G$ at 394 meV) but for most SWNT species, its energy falls outside the laser tuning range (the assignment is therefore not definitive). A third sideband yet to be assigned [s in Fig. 3(a)], appears very close to E_{22} and it cannot be described by a rigid shift with respect to E_{22}.

Two sidebands to E_{11} ($L1$ and $L1^*$) have also been identified and are assigned to continuum or near continuum states. They are both similar in intensity ($\sim 1/10E_{22}$), with linewidth similar to E_{22}. To support the assignment, in Fig. 3(b) the PL energy (E_{11}) is subtracted from the sideband energy, and this energy shift ($X - E_{11}$) is plotted versus inverse diameter. $L1$ shows a linear dependence ($0.45d^{-1}$) with extrapolation to zero. For $L1^*$, we find that a 120 meV energy offset ($0.12 + 0.45d^{-1}$) with respect to $L1$ is most adequate (the linear form $0.57d^{-1}$ cannot de discarded). A plot of $L1$ and $L1^*$ versus E_{11} reveals a weak but clear family pattern, well-reproduced using empirical functional forms [12]. In Fig. 3(b), phonon sidebands would appear as horizontal lines ($2G$ or $G + 2G'$ are expected at 394 and 526 meV, respectively) and so this assignment is excluded. The G-sideband observed recently falls outside our laser tuning range [19,20].

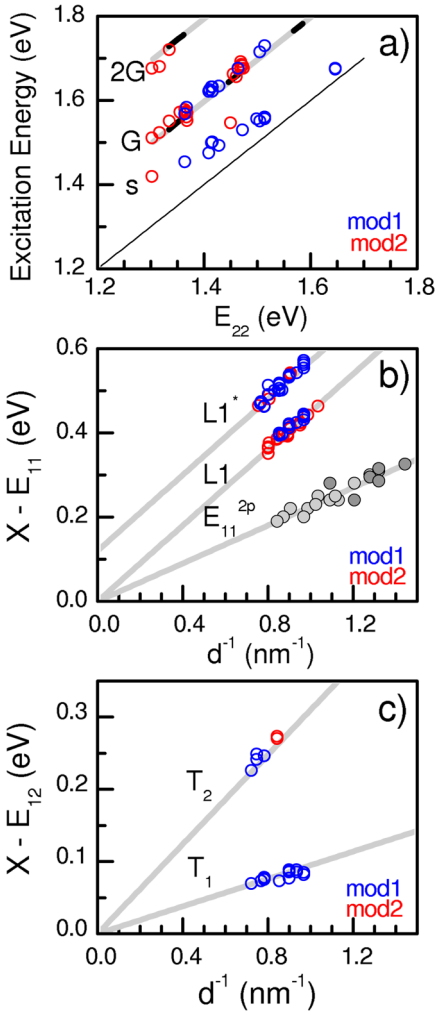

FIG. 3 (color online). Sidebands to E_{22}, E_{11}, and E_{12}. (a) Sideband energy (G, $2G$, and s) versus E_{22} energy. The thin line indicates the E_{22} resonance, and the thick lines are offset from E_{22} by the corresponding phonon energy ($G = 197$ meV). (b) Energy difference between a sideband ($L1$ and $L1^*$) and E_{11} emission versus SWNT inverse diameter. The gray circles are obtained from two-photon excitation experiments [4,21]. The continuous gray lines are linear functional form (see text). (c) Energy difference between a sideband (T_1 and T_2) and E_{12} absorption versus SWNT inverse diameter. The continuous gray lines are linear functional form (see text). Red circles are for mod2 and blue circles for mod1 SWNT species.

The energies of optical excitations, including the two-photon allowed $E_{11}{}^{2p}$ transition (the $2p$ superscript is taken from the Rydberg series) [3,4] scale primarily with SWNT inverse diameter. The data from the two-photon absorption experiment (Refs. [4,21]) are shown as gray circles in Fig. 3(b). Using a hydrogenic model, those authors have estimated the continuum energy (or the ex-

citon binding energy) to be of order of $1.4(E_{11}{}^{2p} - E_{11})$. Both $L1$ and $L1^*$ appear at a significantly higher energy and therefore are not obviously related to the two-photon data [22].

Theory lends some support to the assignment of $L1$ to the continuum but also leads to some apparent inconsistencies. Using the results of Ref. [23] with the same value of γ_o and U as for E_{12}, E_{11}, and E_{22}, we found the continuum to be close to $L1$ energy. However, an empirical model using different parameters appropriate for p-conjugated polymers provides good agreement with estimates from the two-photon experiment [24]. The differences can be explained by the sensitivity of excitonic properties to dielectric screening. In the two-photon experiments, the liquid or solid matrix surrounding the SWNTs screens the Coulomb potential and the exciton binding energy is reduced compared to vacuum. Theoretically, its magnitude should scale as $\epsilon^{-1.4}$ [25]. Using the result of a recent calculation by Capaz *et al.* for SWNTs in vacuum ($\epsilon = 1.846$) [26], the exciton binding energy corresponds well to $L1^*$ resonance. Moreover, using $\epsilon = 3.1$ [26] in the scaling relationship found by Pereibenos *et al.* [25], leads to a good agreement with the two-photon experiment and the calculation by Wang *et al.* [21].

Two sidebands (T_1 and T_2) have also been identified in transverse excitation. Similar to Figs. 3(b) and 3(c) is a plot of the difference between the sideband energy and E_{12} ($X - E_{12}$) versus inverse diameter. T_1 is the weakest of all features assigned in this work, while T_2 is sometimes as strong as E_{12} (for mod2, these sidebands would lie very close to E_{22} and are difficult to observe). The two sidebands are better described with diameter dependence rather than a rigid shift with respect to E_{12}. The linear functional form is shown in Fig. 3(c) ($E_{T1} - E_{12} = 0.095d^{-1}$, $E_{T2} - E_{12} = 0.31d^{-1}$). We do not rigorously assign these resonances. However, similar to E_{11} and E_{22} excitons, the E_{12} exciton should have a related continuum. According to Ref. [16], this continuum is expected close to E_{12}, specifically at 1.08^*E_{12} for $\gamma_o = 2.6$ eV and $U \sim 0.07\gamma_o$. This number falls halfway between T_1 and T_2.

In summary, we used PL imaging to extract several optical excitation resonances in SWNTs, and those resonances were assigned to absorption assisted by phonon or absorption into excited excitonic states. Seven longitudinal and transverse excitonic resonances, namely, E_{11}, $E_{11} + L1$, $E_{11} + L1^*$, E_{12}, $E_{12} + T_1$, E_{22}, and $E_{22} + G$ have now been identified in as many as twenty-five SWNT species, and they all show a family pattern with a specific empirical functional form. Assigning the $L1$ resonance to the continuum, we obtain a diameter dependent binding energy of 450 meV/d (d is the SWNT diameter in nanometer) for E_{11} excitons in SWNTs suspended in free space (alternatively, this number is 120 meV higher if $L1^*$ is assigned to the continuum). The transverse E_{12} transition is identified and its energy is close to E_{22}, in line with the excitonic picture. Comparison with theory allows for an estimate of $\gamma_o = 2.6$ eV and $U \sim 0.07\gamma_o = 0.18$ eV. This detailed spectroscopic study provides further support for excitons in SWNTs.

We thank D. G. Austing for sample preparation, K. Kaminska, J. Bond, and P. Marshall for SWNT synthesis, J. McKee for assistance in the optics laboratory, and H. Tran and P. Chow-Chong for lithography and metallization. Some equipment was funded by the JST-CREST "Nanofactory" grant led by Y. Homma.

[1] M. J. O'Connell *et al.*, Science **297**, 593 (2002).
[2] J. Lefebvre, Y. Homma, and P. Finnie, Phys. Rev. Lett. **90**, 217401 (2003).
[3] F. Wang, G. Dukovic, L. E. Brus, and T. F. Heinz, Science **308**, 838 (2005).
[4] J. Maultzsch *et al.*, Phys. Rev. B **72**, 241402 (2005).
[5] T. Ando, J. Phys. Soc. Jpn. **66**, 1066 (1997).
[6] C. D. Spataru, S. Ismail-Beigi, L. X. Benedict, and S. G. Louie, Phys. Rev. Lett. **92**, 077402 (2004).
[7] E. Chang, G. Bussi, A. Ruini, and E. Molinari, Phys. Rev. Lett. **92**, 196401 (2004).
[8] H. Zhao and S. Mazumdar, Phys. Rev. Lett. **93**, 157402 (2004).
[9] J. Lefebvre, D. G. Austing, J. Bond, and P. Finnie, Nano Lett. **6**, 1603 (2006).
[10] H. Ajiki and T. Ando, Jpn. J. Appl. Phys. Suppl. **34-1**, 107 (1995); Physica (Amsterdam) **B201**, 349 (1994).
[11] Y. Miyauchi, M. Oba, and S. Maruyama, Phys. Rev. B **74**, 205440 (2006).
[12] See EPAPS Document No. E-PRLTAO-98-027717 for a supplementary table and figures. For more information on EPAPS, see http://www.aip.org/pubservs/epaps.html.
[13] S. M. Bachilo *et al.*, Science **298**, 2361 (2002).
[14] J. Lefebvre *et al.*, Phys. Rev. B **69**, 075403 (2004).
[15] R. Saito, G. Dresselhaus, and M. S. Dresselhaus, *Physical Properties of Carbon Nanotubes* (Imperial College, London, 1998).
[16] S. Uryu and T. Ando, Phys. Rev. B **74**, 155411 (2006).
[17] Note: In the formalism used in Ando's papers, $U = 0.2$, in units of $2\pi\gamma/L$. See Ref. [10].
[18] Y. Miyauchi and S. Maruyama, Phys. Rev. B **74**, 035415 (2006).
[19] S. G. Chou *et al.*, Phys. Rev. Lett. **94**, 127402 (2005).
[20] F. Plentz *et al.*, Phys. Rev. Lett. **95**, 247401 (2005).
[21] G. Dukovic *et al.*, Nano Lett. **5**, 2314 (2005).
[22] Note: The shift of $L1$ ($E_{L1} - E_{11}$) corresponds to twice the $E_{11}{}^{2p}$ energy shift ($E_{11}{}^{2p} - E_{11}$). This factor of 2 seems coincidental with the present assignment, but a deeper significance is possible in this or alternative assignments.
[23] T. Ando, J. Phys. Soc. Jpn. **73**, 3351 (2004).
[24] Z. Wang, H. Zhao, and S. Mazumdar, Phys. Rev. B **74**, 195406 (2006).
[25] V. Perebeinos, J. Tersoff, and P. Avouris, Phys. Rev. Lett. **92**, 257402 (2004).
[26] R. B. Capaz *et al.*, Phys. Rev. B **74**, 121401 (2006).